

AFIT/GEO/ENP/93D-04

AD-A273 867



DTIC
S **E** **D**
ELECTE
DEC 17 1993

HUMAN VISUAL SYSTEM ENHANCEMENT OF
RECONSTRUCTED SATELLITE IMAGES

THESIS

James E. Treleaven
Captain, USAF

AFIT/GEO/ENP/93D-04

93-30509



Approved for public release; distribution unlimited

93 12 151 31

**Best
Available
Copy**

HUMAN VISUAL SYSTEM ENHANCEMENT OF
RECONSTRUCTED SATELLITE IMAGES

THESIS

Presented to the Faculty of the School of Engineering
of the Air Force Institute of Technology
Air University
In Partial Fulfillment of the
Requirements for the Degree of
Master of Science in Electrical Engineering

James E. Treleaven, B.S.E.E.
Captain, USAF

15 December, 1993

Accession For	
NTIS	CRA&I <input checked="" type="checkbox"/>
DTIC	TAB <input checked="" type="checkbox"/>
Unannounced <input type="checkbox"/>	
Justification	
By	
Distribution /	
Availability Codes	
Dist	Avail and/or Special
A-1	

Approved for public release; distribution unlimited

DTIC QUALITY INSPECTED 1

Preface

The purpose of this research was to investigate the enhancement of satellite images. The immediate need for this research is to improve intelligence imagery. This research was sponsored by the Phillips Laboratory and contributes to the Air Force's investigation into image enhancement.

In performing this work, I incurred a great deal of debt due to the help of others. First, I wish to thank my thesis advisor, Capt (Dr.) Michael C. Roggemann, for showing me the tricks of the trade. I'd also like to thank the other members of my thesis committee, Dr Byron Welsh and Capt (Dr.) Dennis Ruck. Additional thanks go to Messrs. Dan Zambon and Dave Doak for guiding me through the computer wilderness. My gratitude also goes to the AFIT library staff for their patient assistance in helping me find references.

I further wish to thank my children, Miranda, Ian, and Traci, for never complaining about the many weekends and evenings I was unavailable for taking them to the park. Most importantly, I wish to thank my wife, Annie, for her superb management of our household. Your image needs no enhancement.

James E. Treleaven

Table of Contents

	Page
Preface	ii
List of Figures	vi
List of Tables	vii
Abstract	viii
 I. Introduction	 1-1
1.1 Background	1-1
1.1.1 The Satellite Imaging Problem	1-1
1.1.2 Adaptive Optics	1-2
1.1.3 Software Simulation	1-3
1.2 Problem Statement	1-4
1.3 Research Objectives	1-7
1.4 Research Questions	1-7
1.5 Approach	1-7
1.6 Limitations and Scope	1-7
1.7 Key Results	1-8
1.8 Overview	1-8
 II. Literature Review	 2-1
2.1 Human Visual System Attributes	2-1
2.1.1 Brightness Discrimination	2-1
2.1.2 Edge Processing	2-2
2.2 Human Visual System Model	2-2

	Page
2.2.1 Evidence of Linearity	2-2
2.2.2 Evidence of Nonlinearity	2-4
2.2.3 First Approximation: Linear Model	2-5
2.2.4 Complete Model	2-7
2.3 Quality Assessment	2-7
III. Problem Approach	3-1
3.1 Digital Images	3-1
3.2 Sobel Function	3-1
3.3 Unsharp Masking	3-2
3.4 Histogram Equalization	3-6
3.5 Human Visual System Filter	3-9
3.6 Image Quality Assessment	3-10
3.6.1 Observer's Subjective Fidelity Criterion	3-11
3.6.2 Bandwidth Metric	3-11
3.6.3 Entropy Metric	3-12
3.6.4 Variance Metric	3-12
IV. Results	4-1
4.1 Organization	4-1
4.2 Samples of Enhanced Images	4-1
4.3 Results of Observer's Subjective Fidelity Criterion	4-8
4.4 Results of the Objective Criteria	4-16
4.5 Enhancement Techniques: A Comparison Based On Fidelity Criteria	4-20
V. Conclusion	5-1
5.1 Application of IDL Enhancement Routines	5-1
5.2 Fidelity Criteria	5-2

	Page
5.3 Avenues for Future Research	5-2
5.3.1 Topic: Better Unsharp Masking Technique . .	5-3
5.3.2 Topic: Effects of Lower Photon Count	5-3
5.3.3 Topic: Effects of Lower Atmospheric Coherence Diameter	5-3
5.3.4 Topic: Combining Enhancement Techniques .	5-4
5.3.5 Topic: Inverse Filtering with MTF of the HVS	5-4
Appendix A. Spatial Domain Enhancement	A-1
Appendix B. Human Visual System Filter	B-1
Appendix C. A Better Unsharp Masking Routine	C-1
Bibliography	BIB-1
Vita	VITA-1

List of Figures

Figure	Page
1.1. OCNR5 True Image	1-5
1.2. OCNR5 Reconstructed Image	1-6
2.1. Modulation Transfer Function of a Model of the Human Visual System	2-6
2.2. Model of the Human Visual System	2-7
3.1. Effect of Sobel Operator	3-3
3.2. Effect of Unsharp Masking	3-5
3.3. Histogram Before Histogram Equalization	3-7
3.4. Histogram After Histogram Equalization	3-8
4.1. EORSAT True Image	4-2
4.2. RORSAT True Image	4-3
4.3. Reconstructed Image Prior to HVS Filtering, $r_0 = 7cm$, $\overline{K} = 1e6$	4-4
4.4. Reconstructed Image After HVS Filtering	4-5
4.5. Reconstructed Image Prior to Histogram Equalization, $r_0 = 7cm$, $\overline{K} = 1e4$	4-6
4.6. Reconstructed Image After Histogram Equalization	4-7
4.7. Reconstructed Image Prior to Sobel Function, $r_0 = 10cm$, $\overline{K} = 1e6$	4-9
4.8. Reconstructed Image After Sobel Function	4-10
4.9. Reconstructed Image Prior to Unsharp Masking, $r_0 = 20cm$, $\overline{K} = 1e4$	4-11
4.10. Reconstructed Image After Unsharp Masking	4-12
4.11. Comparison of the Various Enhancement Techniques by the Various Fidelity Criteria	4-21

List of Tables

Table	Page
4.1. Image Capture Simulation and Reconstruction Parameters	4-8
4.2. Key to Subjective Criteria	4-13
4.3. EORSAT Subjective Criteria	4-13
4.4. OCNR5 Subjective Criteria	4-13
4.5. RORSAT Subjective Criteria	4-14
4.6. Effects of HVS Filtering	4-14
4.7. Effects of Histogram Equalization	4-15
4.8. Effects of the Sobel Function	4-15
4.9. Effects of Unsharp Masking	4-16
4.10. EORSAT Bandwidth Metric	4-16
4.11. EORSAT Entropy Metric	4-17
4.12. EORSAT Variance Metric	4-17
4.13. OCNR5 Bandwidth Metric	4-17
4.14. OCNR5 Entropy Metric	4-18
4.15. OCNR5 Variance Metric	4-18
4.16. RORSAT Bandwidth Metric	4-18
4.17. RORSAT Entropy Metric	4-19
4.18. RORSAT Variance Metric	4-19
5.1. Technique Selection Matrix	5-2

Abstract

This research investigated the enhancement of satellite images. The goal was to develop and test a suite of image enhancement software routines to improve the quality of reconstructed images for the human visual system. The primary focus was to enhance satellite features. Enhancement was accomplished in both the spatial domain and the frequency domain. In the spatial domain, routines were developed to enhance image contrast and image edges. In the frequency domain, a routine was developed using research into the human visual system. The transfer function of the human visual system was used to develop a filter for frequency domain enhancement. A data set of images was developed using software to simulate the image degradation caused by atmospheric turbulence and the randomness of the image measurement process. The parameters varied in the simulation were atmospheric coherence diameter and total photon count. The routines were applied to this data set and the results were evaluated by various image fidelity criteria. These criteria included an observer's subjective fidelity criterion as well as objective fidelity criteria. All enhancement routines provided enhancement dependent upon the parameters of the data set simulation. Contrast enhancement worked well when photon count was low. Edge enhancement worked well when photon count was high. The frequency domain filter worked well under all simulation parameters.

HUMAN VISUAL SYSTEM ENHANCEMENT OF RECONSTRUCTED SATELLITE IMAGES

I. Introduction

1.1 Background

1.1.1 The Satellite Imaging Problem. The US Air Force operates several space surveillance sites including the Air Force Maui Optical Station (AMOS), located atop Mt Haleakala on the island of Maui in the state of Hawaii. A 1.6 meter telescope at this site obtains high resolution imagery of space objects, including satellites [20]. Human analysts use this imagery in the development of intelligence estimates.

Satellite imaging comes with a set of problems which are different from those of conventional imaging [2]. First, due to the satellite's relatively great distance from the observatory, good resolution is difficult. If imaging at a wavelength of 500 nm, at a range of 500 km, with a telescope diameter of 1.6 m, theoretical resolution is limited to 19 cm. Second, the rapid motion of a satellite across the sky poses a difficult tracking problem. This limits the length of time during which photons may be collected for a single exposure frame. Finally, the satellite rapidly changes its orientation and its apparent size. These rapid changes limit the time available to collect frames for a given image reconstruction. Multi-frame exposure time is generally on the order of 3 to 10 seconds for satellites within 2,000 km.

Images of satellites taken from the earth suffer from atmospheric turbulence-induced optical aberrations. Turbulence in the atmosphere causes the atmosphere's index of refraction to vary rapidly in space and time [17] [18]. This variation leads to random phase aberrations appearing in the telescope's pupil. Random phase

aberrations cause the optical transfer function (OTF) to be a random process. When compared with the diffraction-limited OTF of a large telescope, the average OTF of an uncompensated telescope is attenuated and approaches zero at relatively low spatial frequencies [18]. This high frequency attenuation means that the limiting resolution of the telescope's imaging system is imposed by the atmosphere rather than by the size of a large telescope. The end result is an image of low resolution and low quality.

1.1.2 Adaptive Optics. An adaptive optics hardware system partially corrects the random phase aberrations caused by atmospheric turbulence [17] [18]. This hardware system includes a wavefront sensor (WFS) and a deformable mirror (DM). The WFS estimates the state of the telescope's generalized pupil function. A reconstruction law maps the WFS measurements into commands for the actuators of the DM. The actuator commands will change the surface of the deformable mirror into an estimate of the conjugate of the phase of the generalized pupil function. When the propagating wave reflects from the DM, the variance of its random phase aberration is reduced. A reduced phase aberration variance means an improved average OTF which means an improved image [18].

The AMOS Compensated Imaging System (CIS) attempts to compensate for the aberrations caused by atmospheric turbulence [20]. The CIS consists of a closed-loop system with wavefront sensor, wavefront computer, and wavefront corrector to remove phase distortions from the wavefront. The wavefront sensor uses two shearing interferometers to measure the slope of the wavefront in two orthogonal directions at 152 discrete subaperture positions. The wavefront computer then uses these slope measurements to calculate the corrections necessary to remove the phase distortions. The turbulence-induced wavefront phase distortion has both tilt error and higher order aberrations. These aberrations are removed by the wavefront correction system. The wavefront correction system consists of a tilt correction mirror and a deformable, monolithic, piezoelectric mirror (DM) with 168 actuators [20]. The tilt correction

mirror uses commands from the wavefront computer to remove wavefront tilt error. The DM uses commands from the wavefront computer to remove the higher order aberrations.

A slow-scan charge-coupled device (CCD) camera captures the compensated image and records it on a hard disk [20]. The images are then processed to further compensate for turbulence effects and, finally, distributed to the end user.

1.1.3 Software Simulation. Michael Roggemann of the Air Force Institute of Technology has developed a suite of software routines written in the FORTRAN programming language which simulate the AMOS image measurement and processing system [19]. As actual satellite imagery from AMOS was unavailable, this suite allowed creation of a data set which closely simulated AMOS imagery. This suite simulated the degradation caused by atmospheric turbulence as well as the efforts of the adaptive optics to compensate for them. In addition, this suite included a linear reconstruction algorithm which produced a reconstructed image by deconvolving the average point spread function from the raw image after averaging [18].

The two components of the adaptive optics simulation of interest to this research are: (1) an adaptive optics component which consists of an atmospheric phase screen generator, a WFS model, a DM model, and a tilt-removal system; and (2) an image simulation component which generates photon-limited images using a user-specified object (satellite) and the user-specified average rate of photoevents. The atmospheric phase screen is modeled as a single thin phase screen in the pupil of the telescope. The phase screen does provide some image degradation.

Tilt-removal was done with a least-squares fit of a plane wave to the phase screen. The plane wave was then subtracted from the phase screen. The phase screen, now without tilt, was input to a Hartmann-type WFS model where phase difference measurements were made. The effects of measurement noise were included. Phase difference measurements were then mapped to DM actuator commands which

compute the position of the surface of the DM. DM phase was then subtracted from the incident random phase and tilt was again removed [19].

The photon-limited images were captured on a 256 x 256 pixel matrix. The object was convolved with the instantaneous point-spread function to obtain the image. This image was normalized and multiplied by the average number of photoevents per image [19]. The image was then postprocessed using a linear image reconstruction algorithm yielding a reconstructed image [18]. This reconstructed image became part of the data set for this research.

A true image, similar to the one in Figure 1.1, is the input object. The true image is a digital representation of an actual satellite. A typical reconstructed image is shown in Figure 1.2. The true image represents the best possible reconstructed image; the reconstructed image is what the intelligence analyst sees. The reconstructed image has poor contrast and undefined features. If the reconstructed image can be made more like the true image, the intelligence analysts job will be easier. Enhancing the features of the reconstructed image is the motivation behind this research.

1.2 Problem Statement

The problem addressed by this thesis is the application of knowledge of the human visual system to develop image enhancement software routines to maximize the transfer of information from the reconstructed image to the human intelligence analyst. These routines encode algorithms which enhance in both the spatial domain as well as in the frequency domain. Knowledge of the human visual system (HVS), including the modulation transfer function (MTF) of the HVS, will be used to develop these algorithms.

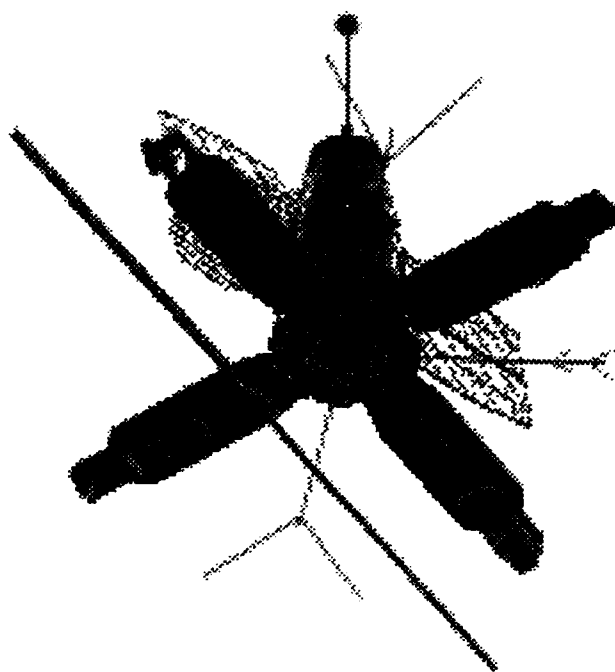


Figure 1.1 OCNr5 True Image

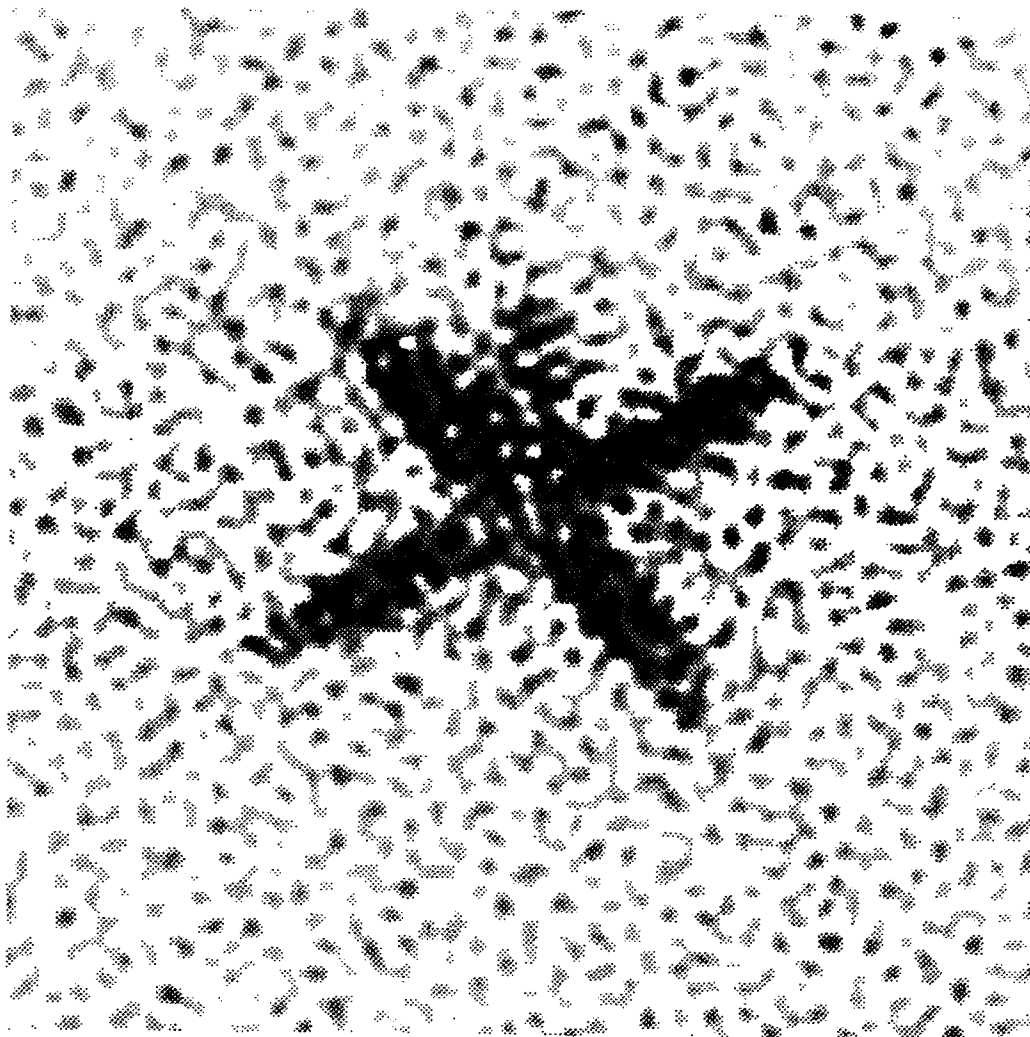


Figure 1.2 OCNR5 Reconstructed Image

1.3 Research Objectives

In this research, a suite of image enhancement software routines which improve the quality of reconstructed satellite images was developed and tested. This suite was transitioned to AMOS, where it will be used to produce better satellite images.

1.4 Research Questions

Here is a list of the key questions this research must answer:

- (1) Can the contrast of a reconstructed satellite image be enhanced?
- (2) Can the edges of a reconstructed satellite image be enhanced?
- (3) Can a useful filter be developed using the MTF of the HVS?
- (4) Do quantitative metrics rank the enhanced images in the same order as the human observer?

1.5 Approach

This project began by creating a database of reconstructed images using Roggemann's software simulation routines with true images as input. Image enhancement software routines were then developed in the Interactive Data Language (IDL). The database was processed by the image enhancement routines. The enhanced images were judged by both qualitative and quantitative metrics.

1.6 Limitations and Scope

This research is limited in scope to the development of enhancement techniques and their subsequent evaluation. The atmospheric phase screen simulation is limited in that it models all effects of phase aberration as a single phase screen located in the pupil of the telescope. Therefore, reconstructed images created by this simulation are isoplanatic. In practice, an actual image has been corrupted by a multitude of phase screens at various altitudes and suffers from nonisoplanatic effects.

1.7 Key Results

Software routines were developed to enhance image contrast and image edges in the spatial domain. In addition, a routine was developed around the MTF of the HVS which allows enhancement in the frequency domain. All routines provided enhancement under at least some conditions of the data set simulation. HVS filtering provided enhancement under all conditions. Histogram equalization worked best on images of low photon count while the edge enhancement techniques of Sobel function and unsharp masking worked best on images of high photon count. Of the quality metrics used to rank the enhancements, the bandwidth and entropy variance metrics come closest to ranking the enhancements in the same order as the human observer.

1.8 Overview

The remainder of this thesis is organized in the following manner. Chapter II is a literature review of relevant material on the human visual system. Chapter III details the problem approach and the enhancement methods used. Chapter IV describes results. A conclusion, as well as a look at future directions, is detailed in Chapter V.

II. Literature Review

2.1 Human Visual System Attributes

2.1.1 Brightness Discrimination. An image is a two-dimensional light intensity function $f(x, y)$, where x and y are spatial coordinates. The brightness of an image at a point is its gray level. Thus, the value of f at a point (x, y) is its gray level [6:6]. A digital image is an image with discrete spatial coordinates as well as discrete brightness values [6:6]. The satellite images enhanced by this research are digital images.

Knowledge of how the human visual system (HVS) discriminates between different brightness levels is fundamental to understanding image enhancement techniques. The HVS can adapt to light intensity from the scotopic threshold (the minimum stimulation required to excite a response) to the glare limit (the point beyond which further stimulation doesn't excite further response). This range can be as much as 10^{10} [6:26]. The human visual system perceives brightness as a logarithmic function of the light intensity incident on the eye. The visual system only operates over a small subrange of its total adaptation range at a time. It cannot operate over its entire range simultaneously. This phenomenon is known as brightness adaptation, and the current sensitivity level is called the brightness adaptation level.

How does the eye discriminate between brightness changes at a specific adaptation level? The Weber ratio describes where an increment of illumination above background illumination becomes discriminable 50 percent of the time. A small Weber ratio means that small intensity changes are discriminable. Small changes are "good" discrimination; large changes are "poor" discrimination because only large intensity changes are discriminable. A plot of Weber ratio versus logarithmic intensity shows that brightness discrimination is best as background illumination increases [6:27]. Thus, when enhancing images for a human viewer, it is desirable to make them bright.

2.1.2 Edge Processing. In the HVS, spatial information is organized into two channels: a lowpass channel and a bandpass channel [7]. The lowpass channel contains information about the contrast across the image. The bandpass channel contains edge information. Because edge information allows us to discriminate objects, edges are the predominant spatial quality of interest. The retina extracts edge information by subtracting the low frequency information (contrast) and amplifying the resulting signal to fill the dynamic range of the optic nerve. This is very similar to the edge enhancement technique of unsharp masking [7]. Thus, when enhancing images for a human viewer, it is desirable to enhance their edges.

2.2 Human Visual System Model

2.2.1 Evidence of Linearity. There has been much research in the past three decades into developing a model of the human visual system. These models are the result of psychophysical experiments. These experiments have determined that the HVS is sensitive to background illumination level and to the spatial frequency content of an image [21]. The current model of the HVS includes both a linear and a nonlinear portion and assumes that the HVS is a shift invariant system [8].

The portion of the HVS up to the photoreceptors, the cones and rods, in the retina can be modelled as a linear system [8]. The validity of a linear model for this portion of the HVS was shown by the following experiment. An observer was shown two sine wave grating transparencies. The first, a reference grating, was of constant contrast and constant spatial frequency. The second, a test grating, was of variable contrast and constant spatial frequency different from the spatial frequency of the reference grating. Thus, there was one reference grating and as many test gratings as there were spatial frequencies to test. The observer was asked to match the contrast of the test grating to that of the reference grating [14:34] [4] [8].

The reference grating had a luminance function

$$F^0(x, y) = A_\omega^0 \cos(\omega_0 y) \quad (2.1)$$

where ω is a particular spatial frequency and A_ω is the amplitude of the luminance.

The test grating had a luminance function

$$F(x, y) = A_\omega \cos(\omega y). \quad (2.2)$$

Since a linear shift invariant system possesses a transfer function $\overline{D}(\omega)$, the perceived brightness of the reference grating would be

$$\phi^0(x, y) = A_\omega^0 \overline{D}(\omega_0) \cos(\omega_0 y) \quad (2.3)$$

and the perceived brightness of the test grating would be

$$\phi(x, y) = A_\omega \overline{D}(\omega) \cos(\omega y). \quad (2.4)$$

Since the observer is equating the apparent brightness of the test grating with that of the reference grating, we have

$$|\phi^0(x, y)| = |\phi(x, y)|. \quad (2.5)$$

Thus,

$$A_\omega^0 \overline{D}(\omega_0) = A_\omega \overline{D}(\omega). \quad (2.6)$$

Finally, the MTF is expressed by

$$\frac{\overline{D}(\omega)}{\overline{D}(\omega_0)} = \frac{A_\omega^0}{A_\omega} \quad (2.7)$$

[4].

There are nonlinear characteristics of the HVS due to a logarithmic transformation at the photoreceptors. In order to keep the model linear, the actual luminance functions used were of the form [4]

$$F(x, y) = \exp(A_\omega \cos(\omega y)). \quad (2.8)$$

If the photoreceptors do a logarithmic transformation on this luminance function [14:36], the photoreceptor output would be

$$G(x, y) = \ln(\exp(A_\omega \cos(\omega y))) = A_\omega \cos(\omega y). \quad (2.9)$$

This input function allows us to assume linearity for the HVS.

2.2.2 Evidence of Nonlinearity. It's believed that near the photoreceptors in the HVS, that is, near the rods and the cones of the retina, the response of the system to intensity variations is nonlinear; specifically, it's logarithmic [14:34]. The literature has many examples of this nonlinearity. Consider that multiple rods on the retina must be stimulated before the stimulus is perceived even though one quantum of light is sufficient to stimulate a single rod [3:25]. Some of the data on the nonlinear portion comes from research into the Limulus, or horseshoe crab, begun in 1932 by Hartline and Graham. In 1970, S.S. Stevens, after replotting the data of Hartline and Graham, concluded that output intensity follows a power law function of input intensity with an exponent of 0.29 [8]. Other nonlinear effects of the HVS show that there is more to perceived brightness than simple intensity. Brightness constancy refers to the fact that an object's brightness tends to remain constant even though its illumination may change [3:281]. Simultaneous contrast is demonstrated by an object which appears darker in front of a light background than it did in front of a dark background even though the light reflected from its surface has not changed [3:277].

2.2.3 First Approximation: Linear Model. If the HVS response to input intensity is logarithmic, the response can be "linearized" if the transfer function is developed with an input of an exponential sine wave [14:36]. With nonlinearities accounted for by developing a transfer function based on an exponential input function, a first approximation model of the HVS is to consider it a linear, time-invariant, and space-invariant (shift-invariant) system [8]. Since the system is assumed to be linear, when the logarithm of an intensity pattern is increased, the system's response should increase proportionally. Optical spatial invariance is a good assumption near the optic axis of the viewer because the area of acute focus, the fovea, is quite small. Since this research is concerned only with single-frame images, time-invariance is not an issue [8].

A linear, shift-invariant model is proposed for the HVS as follows: an image is input to a linear system (the HVS), modified by the system's impulse response function, and displayed at the output (the brain). The modulation transfer function of this linear system is

$$MTF = (0.2 + 0.45f) \exp(-0.18f) \quad (2.10)$$

where f is spatial frequency in cycles/(degree of visual angle subtended) [12]. This transfer function was based upon the work of Mannos and Sakrison [11] and the work of DePalma and Lowry [5] [12]. A plot of this MTF is shown in Figure 2.1. From the plot it can be seen that this model of the HVS has bandpass character.

Since this model is linear and shift-invariant, Fourier techniques may be applied to its analysis. This is fortunate as other researchers have applied Fourier analysis to the HVS. A model assuming that the human brain computes the two-dimensional Fourier transform of input data has been applied to pattern recognition problems [9] [1]. In addition, the Fourier transform domain provides greater efficiency than do the Walsh/Hadamard or Haar transform domains for number of features required

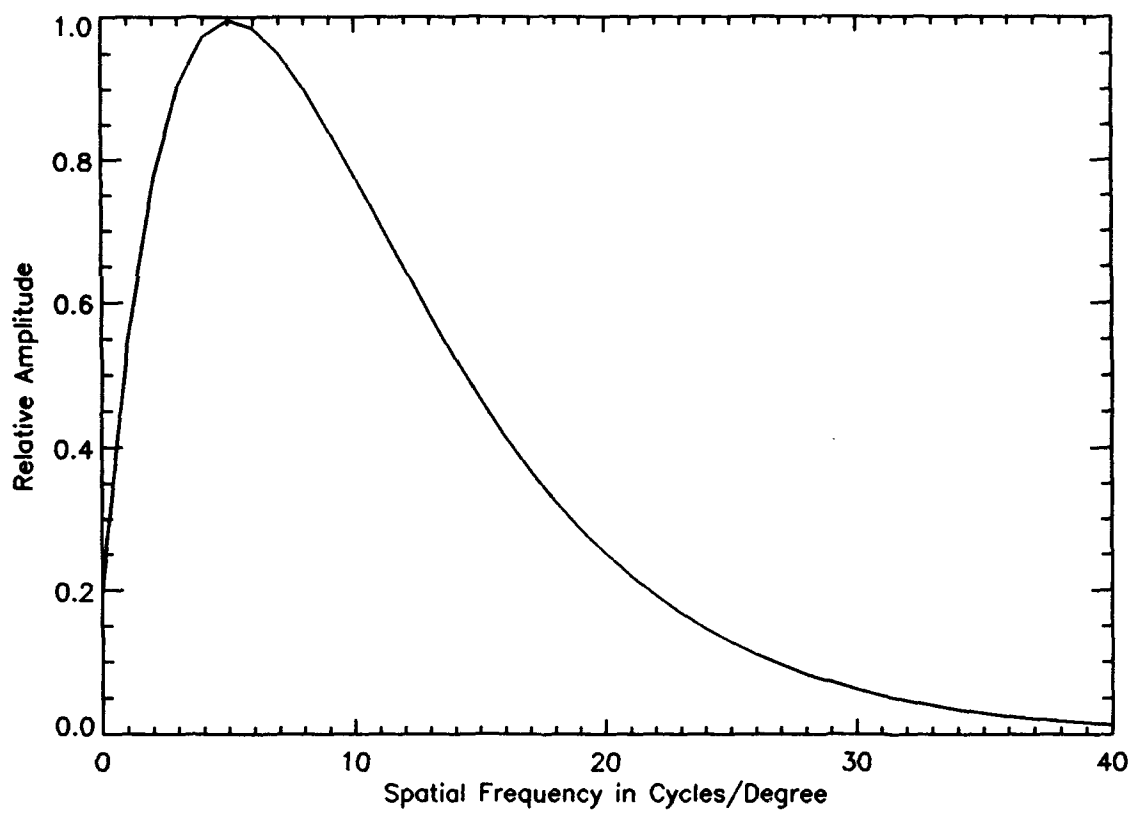


Figure 2.1 Modulation Transfer Function of a Model of the Human Visual System

for minimum mean-square error [8] [1]. This research will enhance images in the frequency domain by taking the Fourier transform of the reconstructed image, multiplying it by the MTF of the HVS, and taking the inverse transform to yield an output image.

2.2.4 Complete Model. A complete model, however, must include the observed nonlinearities. A simple model of the HVS is a logarithmic intensity transform followed by a MTF [8] [14:36]. Such a model is shown in Figure 2.2 [8].

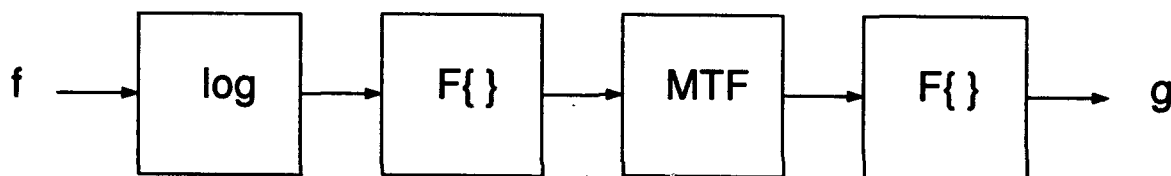


Figure 2.2 Model of the Human Visual System

2.3 Quality Assessment

This chapter closes with a brief mention of image quality assessment. The purpose of image quality assessment is to measure the degree of distortion one can see in the displayed image [7]. The final, and best, judge of image quality is the human image interpreter. Judging the merits of an enhancement routine should involve ranking the enhanced images in order of quality. Any meaningful quantitative fidelity criterion must rank enhanced images in the same order as the end user of the images.

It has been determined that the mean square error (MSE) between the enhanced image and the reconstructed image on a point-by-point basis doesn't correlate well with human quality assessments [12] [7]. This is probably because the HVS doesn't process the image in a point-by-point fashion. Rather, it extracts spatial, temporal, and chromatic features for neural coding [7]. A good quantitative fidelity criterion must properly weight edge fidelity and contrast [7].

III. Problem Approach

This chapter details the enhancement techniques which were applied to the reconstructed images. Two of these techniques, the Sobel function and unsharp masking, enhance edges in the spatial domain. Another, histogram equalization, is used to enhance contrast in the spatial domain. A final technique, filtering based on the human visual system (HVS), is a frequency domain technique. This chapter then concludes with a discussion of the various metrics which were used to evaluate the enhancement techniques. Before explaining the enhancement techniques, it's important to understand the basics of a digital image.

3.1 Digital Images

Recall that an image is a two-dimensional light intensity function $f(i, j)$, where i and j are spatial coordinates. The brightness of an image at a point, $f(i, j)$, is the gray level at that point [6:6]. A digital image has discretized spatial coordinates and brightness values [6:6]. Now, the enhancement techniques used here will be explained in detail.

3.2 Sobel Function

It was pointed out in Chapter 2 that edges are the predominant spatial quality of interest to the human visual system (HVS). Therefore, it's desirable to enhance edges. The Sobel function is one spatial domain enhancement technique which enhances edges. A spatial domain operation which averages pixels over a region, such as the convolution of an object with the point spread function of the system which gives rise to an image, will blur the details of an image. Since averaging is accomplished by integration, differentiation should have the opposite effect of averaging and should sharpen details. Derivative filters accomplish differentiation. Gradients are derivative filters [6:197] and, as such, may be used to enhance edges.

Consider a 3 x 3 image region, or window, as shown in Figure 3.1. The intensity difference between the third and the first column approximates the derivative in the x-direction whereas the intensity difference between the third and the first row approximates the derivative in the y-direction. This window is passed over the entire array. Operations on the border of the array are accomplished by setting the value of all elements on the border to 0. In IDL, the center of the 3 x 3 window, $F(i, j)$, is transformed into $G(i, j)$ by

$$G(i, j) = |x| + |y| \quad (3.1)$$

where

$$x = (A_2 + 2A_3 + A_4) - (A_0 + 2A_7 + A_6) \quad (3.2)$$

and

$$y = (A_0 + 2A_1 + A_2) - (A_6 + 2A_5 + A_4). \quad (3.3)$$

Note that IDL actually implements a fast approximation of a true Sobel function which saves processing time [15:1-221]. The true Sobel function is given by $G(i, j) = \sqrt{x^2 + y^2}$. Figure 3.1 shows an array both before, and after, a Sobel operation. The numbers indicate the gray level of a particular element. Notice that, before the Sobel operation, an edge is visible in which the gray levels are separated by 10. After the Sobel operation, the location of the edge has been emphasized. However, the gray levels are now separated by 40. Thus, the edge has been enhanced. Note that all elements on the edge of the array have been set to 0.

3.3 Unsharp Masking

The purpose of unsharp masking is to highlight fine detail in an image or to enhance detail that has been blurred. All of the test images used for this research have been blurred. In addition, analysts may be interested in the fine details of an image. Recall that details are defined by their edges. Unsharp masking, like the

A0	A1	A2
A7	F(i,j)	A3
A6	A5	A4

3 x 3 Image Region

↙ edge

90	90	100	100	100
90	90	100	100	100
90	90	100	100	100
90	90	100	100	100
90	90	100	100	100

↙ edge

Array Before Sobel

↙ edge

0	0	0	0	0
0	40	40	0	0
0	40	40	0	0
0	40	40	0	0
0	0	0	0	0

↙ edge

Array After Sobel

Figure 3.1 Effect of Sobel Operator

Sobel function, enhances edges. However, it differs from the Sobel function in that it preserves image contrast. Therefore, it would seem like a good candidate to enhance images in need of edge sharpening.

High-boost filtering is the frequency domain equivalent of unsharp masking [6:197]. An understanding of high-boost filtering will give insight into unsharp masking. If a lowpass filtered version of an image is subtracted from the image original, the result is a highpass filtered image. If the original image is multiplied by an amplification factor A , the result is a high-boost filtered image [6:196]:

$$\text{High boost} = (A) \times (\text{Original}) - \text{Lowpass}. \quad (3.4)$$

The high-boost image retains most of the contrast of the original image; however, its edges have been enhanced by removing some of the low spatial frequency content.

Unsharp masking is the spatial domain equivalent of high-boost filtering. The spatial domain equivalent of lowpass filtering is image averaging. This has the effect of blurring the image. The image is first blurred by a boxcar window whose width is operator specified. The boxcar width in pixels, w , must be an odd number smaller than the smallest dimension of the array to be blurred. Each row of w pixels is summed and then divided by w to yield an average. Then, the row results are summed and divided by w to yield the new value for the pixel in the middle of the array. As an example, consider the array shown in Figure 3.2. An edge is clearly visible with opposing elements separated by 11. The blurring algorithm leaves all the elements on the border unchanged. Here, $w = 3$. After blurring, the opposing elements of the edge are only separated by about 6. But, after subtraction from a scaled version of the original, the opposing elements of the edge are separated by 16, an increase of 5 gray levels. Also, note the most of the contrast of the original image has been retained.

80	82	89	100	103	106
81	87	89	100	102	104
86	83	89	100	101	103
83	86	89	100	107	104
84	86	89	100	103	102
81	87	89	100	105	107

INPUT

edge 

80	82	89	100	103	106
81	85	91	97	102	104
86	85	91	97	102	103
83	86	91	97	102	104
84	86	91	98	103	102
81	87	89	100	105	107

INPUT BLURRED
WITH 3X3 WINDOW

edge 

80	82	89	100	103	106
81	89	87	103	102	104
86	81	87	103	100	103
83	86	87	103	112	104
84	86	87	102	103	102
81	87	89	100	105	107

OUTPUT =
(2XINPUT) -- BLUR

edge 

Figure 3.2 Effect of Unsharp Masking

3.4 Histogram Equalization

The goal of histogram equalization is to increase image contrast by increasing the dynamic range of gray levels. Many of the test images used for this research had poor contrast. Therefore, histogram equalization would be a good candidate to enhance images in need of contrast enhancement.

Let the variable r_k represent the k th gray level of the image to be enhanced. The gray levels are in the interval $[0, L - 1]$ with L being the number of possible gray levels. Thus, L is 256 for 8-bit color. We find a transform

$$s_k = T(r_k) \quad (3.5)$$

which gives a new gray level s_k for each gray level r_k of the original image. The transformation function, $T(r_k)$, must satisfy the following conditions:

- (a) $T(r_k)$ must be single-valued and must monotonically increase on the interval $0 \leq r_k \leq L - 1$ and
- (b) $0 \leq T(r_k) \leq L - 1$ for $0 \leq r_k \leq L - 1$.

The first condition preserves the order from black to white in the gray scale. The second condition insures that the new gray scale mapping is consistent with the allowed values of the gray scale [6:173-180].

A transformation function meeting the above conditions is the discrete cumulative distribution function, given by

$$s_k = T(r_k) = \sum_{j=0}^k n_j / n \quad (3.6)$$

$$= \sum_{j=0}^k p_r(r_j) \quad (3.7)$$

for $0 \leq r_k \leq L - 1$ and $k = 0, 1, \dots, L - 1$. In the above equations, n_j is the number of times the j th gray level appears in an image, n is the total number of elements in

an image, and $p_r(r_j)$ is the probability of the k th gray level. This transformation produces an image whose gray levels have a uniform density. This uniform density means an increase in the dynamic range of the pixels which increases image contrast [6:173-180].

IDL accomplishes histogram equalization by first employing the histogram function to obtain the density distribution of the input array. The histogram is integrated yielding the cumulative density-probability function. The color table lookup function then transforms the input array to the output image [16]. Examples of histograms before and after equalization are shown in Figures 3.3 and 3.4.

3.5 Human Visual System Filter

The enhancement techniques discussed thus far have been accomplished in the spatial domain. Enhancement can also be accomplished in the frequency domain. This is a straightforward process of computing the Fourier transform of the image to be enhanced, multiplying it by a filter transfer function, and taking the inverse transform to yield the enhanced image.

As discussed in chapter 2, the HVS is sensitive to certain spatial frequencies. The modulation transfer function (MTF) of the HVS has a bandpass character. If the spectrum of an image is filtered by this MTF, the output spectrum will contain mostly those frequency components of interest to the HVS. Thus, the image will be enhanced.

In the Nill model of the HVS MTF, spatial frequency is expressed in units of cycles/degree [12]. As IDL expresses spatial frequency in units of pixels, it was necessary to modify the Nill model so that the peak transfer would be 1.0 and so the operator could control filter center frequency, bandwidth, and order. Therefore, the modified Nill model will be

$$MTF = (0.52 + 0.45(f/f_c)) \exp(-(z^{2(\text{order})})), \quad (3.8)$$

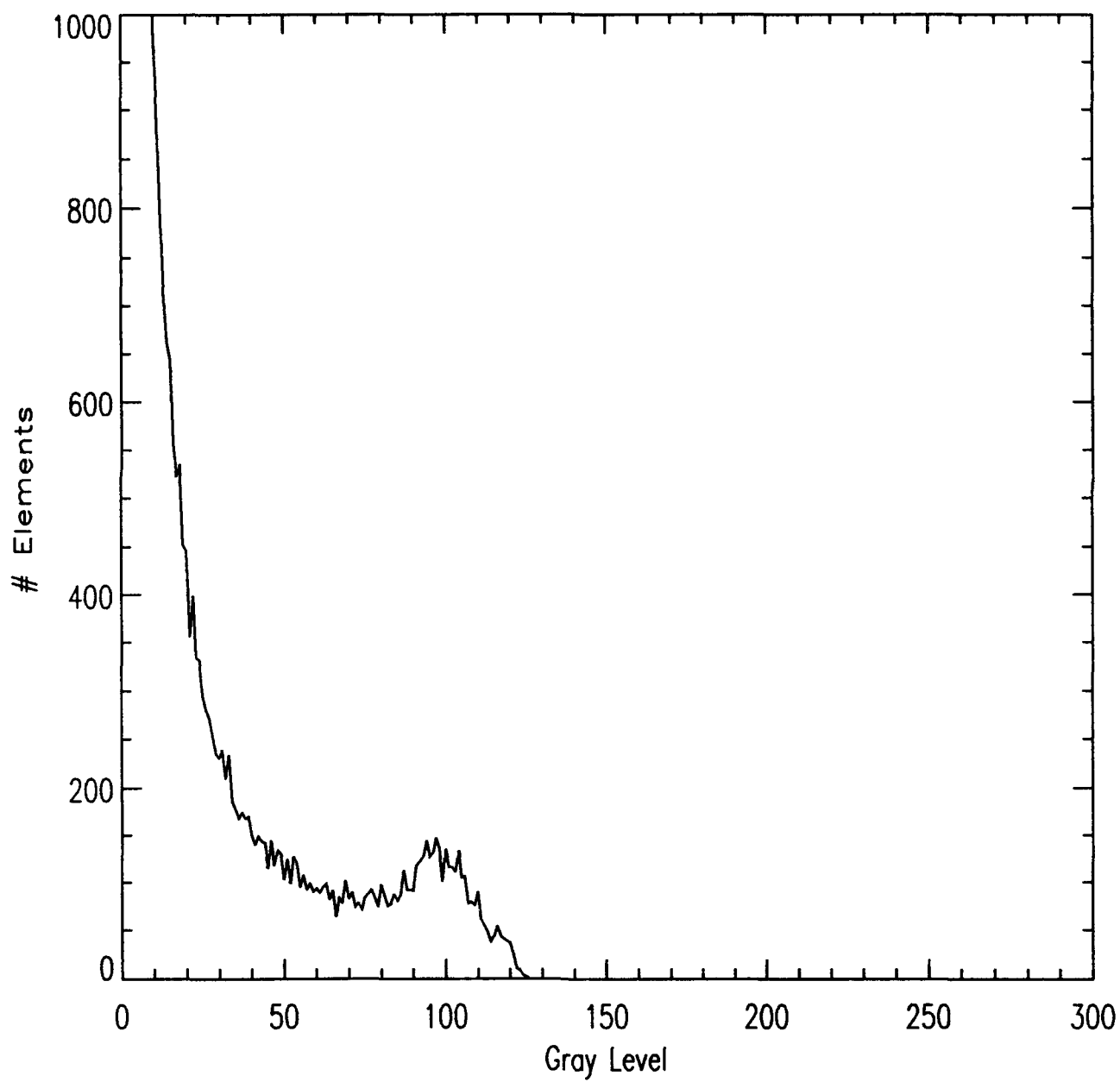


Figure 3.3 Histogram Before Histogram Equalization

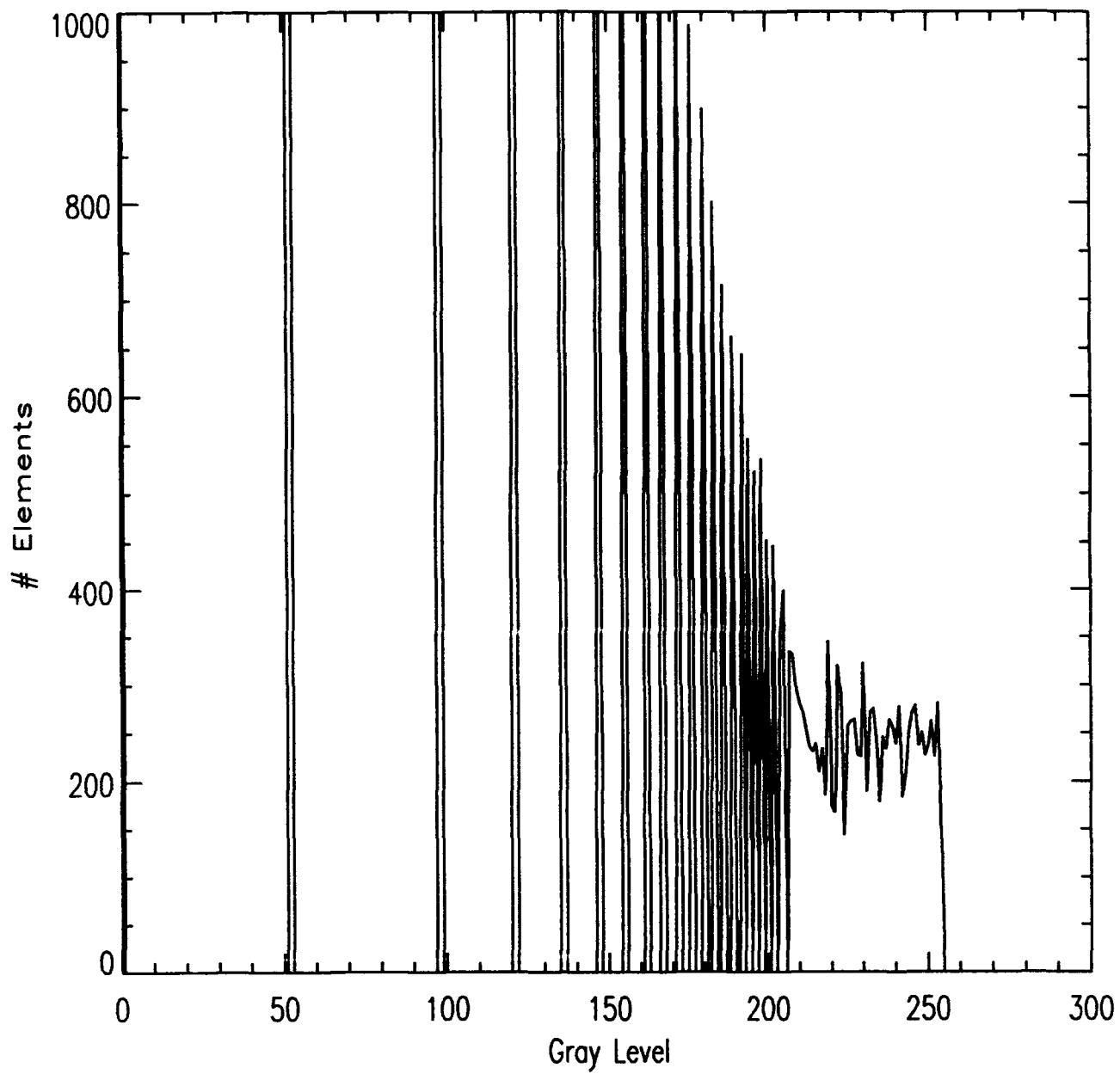


Figure 3.4 Histogram After Histogram Equalization

where f , the spatial frequency, is given by:

$$f = \sqrt{i^2 + j^2}, \quad (3.9)$$

and z , a variable controlling filter roll-off, is given by:

$$z = \frac{f^2 - f_c^2}{f \times bw}. \quad (3.10)$$

Also included in the expression are f_c , the desired filter center frequency; *order*, the filter order; i , a row counter; j , a column counter; and bw , the desired filter bandwidth. This model allows the operator to manipulate filter center frequency from 0 to 96, filter order from 1 to 10, and filter bandwidth from 0 to 48. The parameter limits for center frequency and bandwidth were chosen to keep the filter realization within the spatial frequency limit in IDL of 181. Filter order was limited to 10, because at 10 it already has ideal character.

Let I_r be the Fourier transform of the reconstructed image, I_e be the Fourier transform of the enhanced image. Then, I_e is given by:

$$I_e = I_r \times MTF. \quad (3.11)$$

The output image, i_e , is simply the inverse Fourier transform of I_e .

3.6 Image Quality Assessment

The quality of images is assessed through fidelity criteria. A subjective fidelity criterion is the measurement of image quality through the subjective evaluations of a human observer [6:319–320]. An objective fidelity criterion measures the information lost (sometimes called “error”) between the input and output images [6:319–320]. The enhancement techniques investigated here were evaluated by both subjective and objective fidelity criteria. The fidelity criteria applied to the enhanced images include

an observer's subjective criterion as well as the objective criteria of bandwidth, entropy, and variance. All images subjected to the objective criteria are first cutout from their background. This is accomplished by first determining the location of all elements in the array of the true image that are part of the satellite. These elements are then set to 1 and the others to 0. This new array is then multiplied by the enhanced array with the result being an enhanced satellite on a 0 gray level background. In this manner, only the enhancement of the satellite is considered rather than its background. The remainder of this section describes these criteria.

3.6.1 Observer's Subjective Fidelity Criterion. This is simply an observer's ranking of the best enhancement technique for a given data set. There was only one observer used: the author. The observer was given a true image to compare to the data set. "Best," as used here, applies to the image showing the features of the true image most clearly. Each data set included the true image, the reconstructed image, and an image enhanced by each of the enhancement techniques HVS MTF filtering, histogram equalization, sobel function, and unsharp masking.

3.6.2 Bandwidth Metric. The motivation behind this metric is to measure the energy in the image spectrum within the bandpass of the HVS MTF [13]. In order to make a meaningful comparison between the reconstructed image and the enhanced image, the energy of the two images must be normalized. Also, because the volume of data points in a 2-D spectrum is huge, and because it is difficult to compare a 3-D surface, the image spectra are radially averaged [13]. The radially averaged spectrum is [10]:

$$F_{radavg}(\rho) = \frac{\sum_{\theta} F(\rho, \theta)}{\text{number of pixels at distance } \rho}, \quad (3.12)$$

where $F(\rho, \theta)$ is the modulus of the discrete two-dimensional Fourier transform of $f_{norm}(x, y)$, in polar coordinates with $\rho = \sqrt{u^2 + v^2}$, where u and v are the spatial

domain transforms of x and y . In simple terms, the FFT modulus is shifted so that its zero frequency origin is in the center pixel quad of the array.

The bandwidth metric becomes:

$$BW = \sum_{\rho=\rho_{lower}}^{\rho_{upper}} |F_{rad\ avg}(\rho)|, \quad (3.13)$$

where the ρ_{lower} and ρ_{upper} are determined empirically to fall into the bandpass of the HVS.

3.6.3 Entropy Metric. In information theory, entropy is defined as the average information per source output [6:326]. Entropy yields the average amount of information of the source [6:326]. It is synonymous with uncertainty and as the magnitude of entropy increases, more information is associated with the source [6:326]. For this research, the source is the image. Thus, as the magnitude of entropy in the image increases, there is more uncertainty and, hence, more information in the image. Therefore, a good image should have high entropy.

Entropy is defined by the equation:

$$entropy = - \sum_{j=1}^J P(\nu_j) \log P(\nu_j) \quad (3.14)$$

where ν_j is the gray level of a particular element [6:326]. $P(\nu_j)$ is the probability density function, or histogram, of the gray levels in an image. This number was compared with the entropy of the reconstructed image to see whether the enhancement technique increased the information of the image.

3.6.4 Variance Metric. This metric computes the variance of the image. It gives an idea of how much the gray levels stray from their mean. This can be thought of as the uncertainty in the image. Just as for entropy, a good image should have high entropy.

This metric is computed from the square of the standard deviation of the image and, as such, is object dependent. The algorithm is:

$$\textit{variance} = (\textit{normalized image standard deviation})^2. \quad (3.15)$$

IV. Results

4.1 Organization

The enhancement techniques of human visual system (HVS) filtering, histogram equalization, Sobel function, and unsharp masking, are applied to a matrix of reconstructed images. The fixed parameters of these simulations are shown in Table 4.1. The images are of three Soviet satellites: the Electro-optic Research Satellite (EORSAT), shown in Figure 4.1, the Ocean Research 5 (OCNR5) satellite, shown in Figure 1.1, and the Radar Ocean Research Satellite (RORSAT), shown in Figure 4.2. The variable parameters of these simulations are the atmospheric coherence diameter (r_0) and the total number of photons per image (\bar{K}).

The remainder of this chapter shows samples of enhanced images, discusses the results of the observer's subjective fidelity criterion as well as the various objective criteria, and closes with a comparison of the enhancement techniques.

4.2 Samples of Enhanced Images

The primary motivation behind this research is to make the reconstructed images look more like the true images. This section shows examples of enhanced images for each of the enhancement techniques. Figure 4.3 shows a reconstructed image for a simulation of $r_0 = 7cm$ and $\bar{K} = 10^6$. Figure 4.4 shows this same image after HVS filtering. Note that the solar panels and the antenna have been sharpened.

Figure 4.5 shows a reconstructed image for a simulation of $r_0 = 7cm$ and $\bar{K} = 10^4$. Figure 4.6 shows this same image after histogram equalization. Note that image contrast has been enhanced.

Figure 4.7 shows a reconstructed image for a simulation of $r_0 = 10cm$ and $\bar{K} = 10^6$. Figure 4.8 shows this same image after the Sobel function. Note that the



Figure 4.1 EORSAT True Image



Figure 4.2 RORSAT True Image



Figure 4.3 Reconstructed Image Prior to HVS Filtering, $r_0 = 7cm$, $\overline{K} = 1e6$

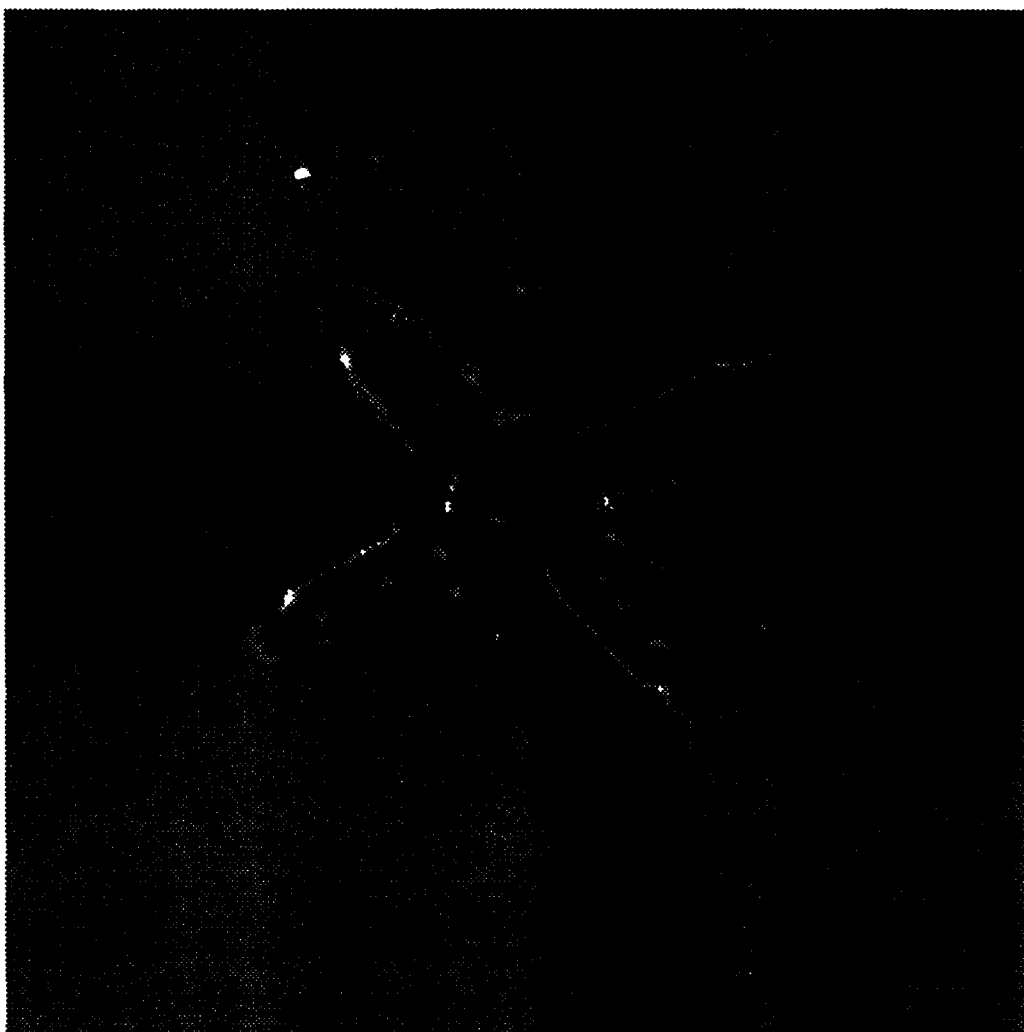


Figure 4.4 Reconstructed Image After HVS Filtering

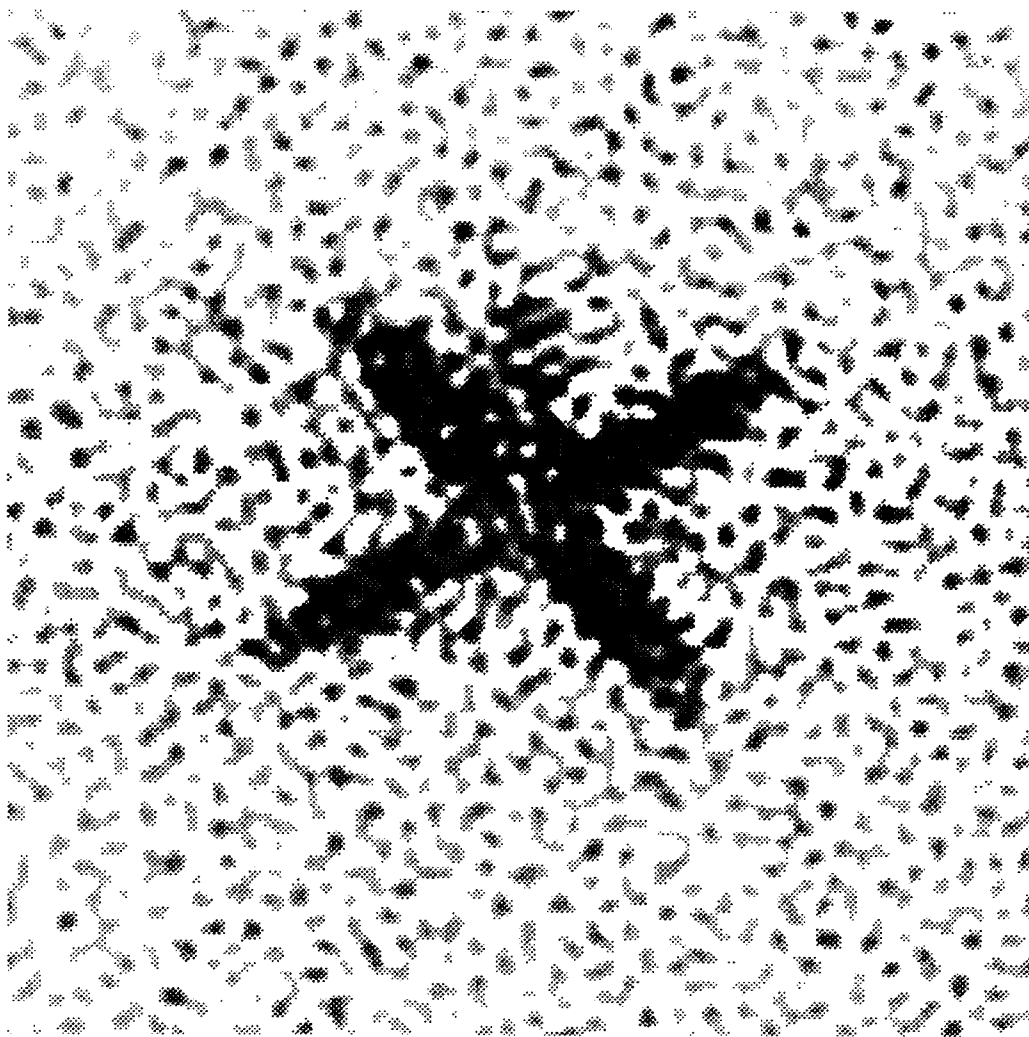


Figure 4.5 Reconstructed Image Prior to Histogram Equalization, $r_0 = 7cm$, $\overline{K} = 1e4$

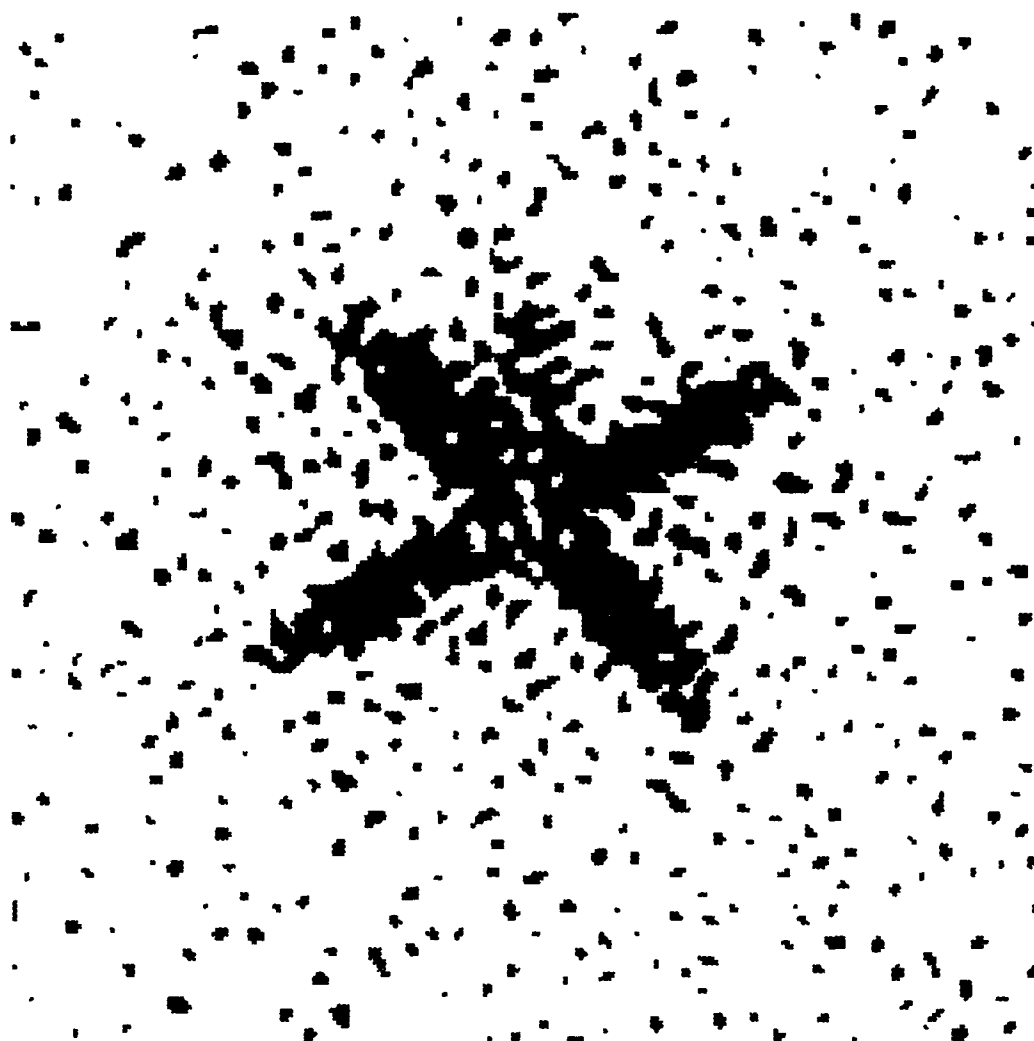


Figure 4.6 Reconstructed Image After Histogram Equalization

Table 4.1 Image Capture Simulation and Reconstruction Parameters

number of frames	100
max no. subaps across max dim of mirror	10
mirror diameter	1.0 m
obscuration diameter	0.0
wavelength	500 nm
target distance	500 km
ccd camera noise variance (photons/pixel)	50
partial compensation imaging	no
correct tilt	yes
use adaptive optics	yes
no. of steps for integration on subap.	20.0
actuator separation grid size in pupil	11 cm
avg no. of pho.events/subap/integ. time	100.0
length of one side of object array	12.0 m
radius of of in pixels	126
wiener filter	no
width of mtf in pixels	45

satellite's edges have been enhanced. Also note that some of the contrast has been lost. This is a negative effect of the Sobel function.

Figure 4.9 shows a reconstructed image for a simulation of $r_0 = 20\text{cm}$ and $\bar{K} = 10^4$. Figure 4.9 shows this same image after unsharp masking. The original image was scaled by 2 and the blurring was done with a 7×7 pixel window. Note that the satellite's edges have been enhanced. Also note that most of the contrast has been retained. This is an advantage over the Sobel function.

4.3 Results of Observer's Subjective Fidelity Criterion

These techniques are evaluated using the observer's subjective fidelity criterion. Each enhancement technique is compared to the reconstructed image. The observer is forced to judge the merits of the technique based on the criteria in Table 4.2. The results of this evaluation are shown in Tables 4.3, 4.4, and 4.5. The unsharp masking enhancement technique produced no image for the OCNR5 reconstructed satellite



Figure 4.7 Reconstructed Image Prior to Sobel Function, $r_0 = 10cm$, $\bar{K} = 1e6$

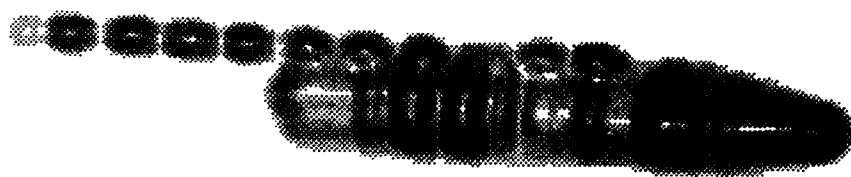


Figure 4.8 Reconstructed Image After Sobel Function

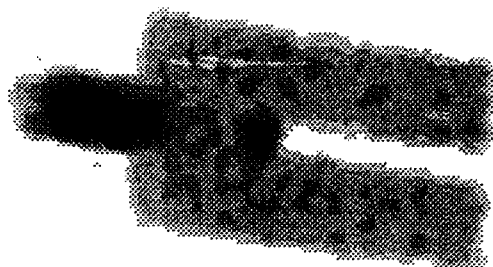


Figure 4.9 Reconstructed Image Prior to Unsharp Masking, $r_0 = 20cm$, $\bar{K} = 1e4$

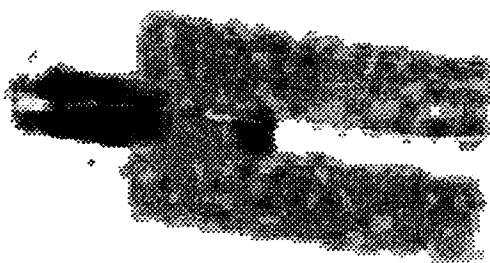


Figure 4.10 Reconstructed Image After Unsharp Masking

Table 4.2 Key to Subjective Criteria

r_0	atmosphere coherence diameter, meters
\bar{K}	average number of photons per image
+	Technique definitely sharpened some feature.
0	Technique neither sharpened nor blurred image.
-	Technique blurred overall image.

with simulation parameters of $r_0 = 0.2$ and $\bar{K} = 10^4$. It so happens that with a smoothing window of 7 pixels, the smoothed array is almost equal to the input array and their difference is zero. This gave a maximum intensity of zero for the unsharp masking technique. When the smoothing window was increased to 49 pixels, the maximum intensity for the unsharp masked image was 2.0. (Note: The asterisk in a table indicates that the image was unavailable for evaluation.)

Table 4.3 EORSAT Subjective Criteria

Enhancement Technique	$r_0 = 0.2$		$r_0 = 0.1$		$r_0 = 0.07$	
	$\bar{K} = 1e6$	$\bar{K} = 1e4$	$\bar{K} = 1e6$	$\bar{K} = 1e4$	$\bar{K} = 1e6$	$\bar{K} = 1e4$
HVS filtering	+	+	+	+	+	0
histogram equalization	-	-	-	-	-	+
sobel function	+	-	-	-	-	+
unsharp masking	+	-	-	-	+	-

Table 4.4 OCNR5 Subjective Criteria

Enhancement Technique	$r_0 = 0.2$		$r_0 = 0.1$		$r_0 = 0.07$	
	$\bar{K} = 1e6$	$\bar{K} = 1e4$	$\bar{K} = 1e6$	$\bar{K} = 1e4$	$\bar{K} = 1e6$	$\bar{K} = 1e4$
HVS filtering	+	+	+	+	+	+
histogram equalization	+	-	+	-	+	+
sobel function	+	-	+	-	+	-
unsharp masking	+	*	+	-	+	-

Table 4.5 RORSAT Subjective Criteria

Enhancement Technique	$r_0 = 0.2$		$r_0 = 0.1$		$r_0 = 0.07$	
	$K = 1e6$	$K = 1e4$	$K = 1e6$	$K = 1e4$	$K = 1e6$	$K = 1e4$
HVS filtering	+	+	+	+	+	+
histogram equalization	-	-	-	+	-	+
sobel function	+	-	+	+	+	-
unsharp masking	+	-	+	-	+	-

Table 4.6 Effects of HVS Filtering

	$K = 1e6$	$K = 1e4$
EORSAT, $r_0 = 0.2$	+	+
EORSAT, $r_0 = 0.1$	+	+
EORSAT, $r_0 = 0.07$	+	0
OCNR5, $r_0 = 0.2$	+	+
OCNR5, $r_0 = 0.1$	+	+
OCNR5, $r_0 = 0.07$	+	+
RORSAT, $r_0 = 0.2$	+	+
RORSAT, $r_0 = 0.1$	+	+
RORSAT, $r_0 = 0.07$	+	+

As Tables 4.3, 4.4, and 4.5 show, all of the enhancement techniques provide enhancement under some conditions. HVS filtering, however, provides enhancement regardless of conditions as shown in Table 4.6.

Describing the conditions under which histogram equalization may be usefully employed is not as clear as for HVS filtering. As Table 4.7 shows, histogram equalization is more often successful (four of nine cases as opposed to three of nine cases) in enhancement under conditions of low photon count. The usefulness of histogram equalization under differing values of r_0 is undetermined by this data. It would be interesting to determine whether histogram equalization provides enhancement under very low atmospheric coherence diameters, r_0 .

The Sobel function and unsharp masking are useful under conditions of high photon count as shown in Tables 4.8 and 4.9. All of the unsharp masked images

Table 4.7 Effects of Histogram Equalization

	$K = 1e6$	$K = 1e4$
EORSAT, $r_0 = 0.2$	-	-
EORSAT, $r_0 = 0.1$	-	-
EORSAT, $r_0 = 0.07$	-	+
OCNR5, $r_0 = 0.2$	+	-
OCNR5, $r_0 = 0.1$	+	-
OCNR5, $r_0 = 0.07$	+	+
RORSAT, $r_0 = 0.2$	-	-
RORSAT, $r_0 = 0.1$	-	+
RORSAT, $r_0 = 0.07$	-	+

Table 4.8 Effects of the Sobel Function

	$K = 1e6$	$K = 1e4$
EORSAT, $r_0 = 0.2$	+	-
EORSAT, $r_0 = 0.1$	-	-
EORSAT, $r_0 = 0.07$	-	+
OCNR5, $r_0 = 0.2$	+	-
OCNR5, $r_0 = 0.1$	+	-
OCNR5, $r_0 = 0.07$	+	-
RORSAT, $r_0 = 0.2$	+	-
RORSAT, $r_0 = 0.1$	+	+
RORSAT, $r_0 = 0.07$	+	-

were enhanced by subtracting an array smoothed with a 7 x 7 pixel window from an unscaled input array. Different smoothing windows weren't explored. One attempt was made to scale the input array by 2 and the pleasing result, at least in contrast, is shown in Figure 4.9. Also, as is the case for histogram equalization, the usefulness of the Sobel function and of unsharp masking under differing values of r_0 is undetermined by this data. It would be interesting to determine whether these techniques provide enhancement under very low atmospheric coherence diameters, r_0 .

Table 4.9 Effects of Unsharp Masking

	$\bar{K} = 1e6$	$\bar{K} = 1e4$
EORSAT, $r_0 = 0.2$	+	-
EORSAT, $r_0 = 0.1$	-	-
EORSAT, $r_0 = 0.07$	+	-
OCNR5, $r_0 = 0.2$	+	*
OCNR5, $r_0 = 0.1$	+	-
OCNR5, $r_0 = 0.07$	+	-
RORSAT, $r_0 = 0.2$	+	-
RORSAT, $r_0 = 0.1$	+	-
RORSAT, $r_0 = 0.07$	+	-

Table 4.10 EORSAT Bandwidth Metric

	$r_0 = 0.2$		$r_0 = 0.1$		$r_0 = 0.07$	
Enhancement Technique	$\bar{K} = 1e6$	$\bar{K} = 1e4$	$\bar{K} = 1e6$	$\bar{K} = 1e4$	$\bar{K} = 1e6$	$\bar{K} = 1e4$
Reconstructed Image	.367	.366	.368	.358	.369	.345
HVS filtering	.388	.350	.424	.420	.454	.338
Histogram Equalization	.280	.296	.279	.282	.279	.269
Sobel Function	.373	.331	.370	.274	.365	.260
Unsharp Masking	.308	.303	.318	.283	.323	.191

4.4 Results of the Objective Criteria

In this section, the results of applying the objective criteria of bandwidth, entropy, and variance to the enhancements of the reconstructed images are presented. This criteria was described in Chapter 3. Recall that, for all of the objective criteria, the higher these numbers are, the better the metric considers the enhancement to be. For reasons cited in the previous section, the unsharp masking enhancement technique produced no image for the OCNR5 reconstructed satellite with simulation parameters of $r_0 = 0.2$ and $\bar{K} = 10^4$. (Note: The asterisk in a table indicates that the image was unavailable for evaluation.)

Table 4.11 EORSAT Entropy Metric

Enhancement Technique	$r_0 = 0.2$		$r_0 = 0.1$		$r_0 = 0.07$	
	$K = 1e6$	$K = 1e4$	$K = 1e6$	$K = 1e4$	$K = 1e6$	$K = 1e4$
Reconstructed Image	.819	.848	.826	.869	.844	.862
HVS Filtering	.864	.889	.865	.904	.886	.943
Histogram Equalization	.869	.484	.870	.498	.860	.480
Sobel Function	.725	.327	.757	.440	.824	.566
Unsharp Masking	.683	.023	.701	.026	.747	.139

Table 4.12 EORSAT Variance Metric

Enhancement Technique	$r_0 = 0.2$		$r_0 = 0.1$		$r_0 = 0.07$	
	$K = 1e6$	$K = 1e4$	$K = 1e6$	$K = 1e4$	$K = 1e6$	$K = 1e4$
Reconstructed Image	43	44	43	45	43	49
HVS Filtering	585	811	410	395	325	154
Histogram Equalization	28	35	28	35	28	36
Sobel Function	88	79	87	53	78	42
Unsharp Masking	722	2058	674	1936	625	4829

Table 4.13 OCNR5 Bandwidth Metric

Enhancement Technique	$r_0 = 0.2$		$r_0 = 0.1$		$r_0 = 0.07$	
	$K = 1e6$	$K = 1e4$	$K = 1e6$	$K = 1e4$	$K = 1e6$	$K = 1e4$
Reconstructed Image	.358	.357	.359	.342	.358	.318
HVS filtering	.258	.435	.454	.426	.313	.491
Histogram Equalization	.295	.362	.293	.343	.287	.304
Sobel Function	.277	.254	.277	.251	.274	.274
Unsharp Masking	.279	*	.282	.151	.267	.110

Table 4.14 OCNR5 Entropy Metric

Enhancement Technique	$r_0 = 0.2$		$r_0 = 0.1$		$r_0 = 0.07$	
	$K = 1e6$	$K = 1e4$	$K = 1e6$	$K = 1e4$	$K = 1e6$	$K = 1e4$
Reconstructed Image	1.28	1.26	1.27	1.22	1.27	1.13
HVS Filtering	1.27	1.31	1.30	1.29	1.28	1.30
Histogram Equalization	1.16	0.51	1.15	0.51	1.16	0.51
Sobel Function	1.23	0.40	1.23	0.49	1.23	0.64
Unsharp Masking	0.95	*	0.94	0.01	0.97	0.14

Table 4.15 OCNR5 Variance Metric

Enhancement Technique	$r_0 = 0.2$		$r_0 = 0.1$		$r_0 = 0.07$	
	$K = 1e6$	$K = 1e4$	$K = 1e6$	$K = 1e4$	$K = 1e6$	$K = 1e4$
Reconstructed Image	26	27	26	28	27	32
HVS Filtering	453	92	69	106	269	55
Histogram Equalization	21	32	21	32	21	31
Sobel Function	36	46	35	38	35	33
Unsharp Masking	136	*	131	7149	155	3470

Table 4.16 RORSAT Bandwidth Metric

Enhancement Technique	$r_0 = 0.2$		$r_0 = 0.1$		$r_0 = 0.07$	
	$K = 1e6$	$K = 1e4$	$K = 1e6$	$K = 1e4$	$K = 1e6$	$K = 1e4$
Reconstructed Image	.426	.425	.426	.420	.424	.395
HVS filtering	.406	.450	.381	.424	.409	.3307
Histogram Equalization	.324	.381	.323	.373	.326	.3312
Sobel Function	.355	.334	.356	.332	.355	.294
Unsharp Masking	.289	.247	.288	.211	.291	.161

Table 4.17 RORSAT Entropy Metric

Enhancement Technique	$r_0 = 0.2$		$r_0 = 0.1$		$r_0 = 0.07$	
	$K = 1e6$	$K = 1e4$	$K = 1e6$	$K = 1e4$	$K = 1e6$	$K = 1e4$
Reconstructed Image	.615	.614	.616	.610	.614	.586
HVS Filtering	.639	.632	.638	.626	.639	.627
Histogram Equalization	.553	.393	.551	.385	.528	.366
Sobel Function	.620	.369	.619	.373	.619	.406
Unsharp Masking	.573	.030	.578	.045	.567	.136

Table 4.18 RORSAT Variance Metric

Enhancement Technique	$r_0 = 0.2$		$r_0 = 0.1$		$r_0 = 0.07$	
	$K = 1e6$	$K = 1e4$	$K = 1e6$	$K = 1e4$	$K = 1e6$	$K = 1e4$
Reconstructed Image	68	69	68	69	27	74
HVS Filtering	1961	238	7219	300	269	1770
Histogram Equalization	49	59	49	59	21	58
Sobel Function	65	66	65	69	35	66
Unsharp Masking	1438	845	1595	1719	155	3970

4.5 Enhancement Techniques: A Comparison Based On Fidelity Criteria

It is desirable to compare each fidelity criterion's evaluation of each enhancement technique. Therefore, points are assigned to each evaluation as follows. Each criterion is forced to rank the enhancements for a given realization of a given satellite. Since there are four enhancements for each realization, they are ranked first through fourth. The observer ranked the enhancements subjectively. The other criteria ranked an image first if it had the highest numerical evaluation and fourth if it had the lowest. First is given 4 points, second is given 3 points, third is given 2 points, and fourth is given 1 point. The points are then totalled for each enhancement technique. The comparison is shown in Figure 4.11.

This figure shows that, regardless of fidelity criteria, HVS filtering consistently provided the best enhancement. The subjective criteria, bandwidth metric, and entropy metric considered histogram equalization and the Sobel function to be on a par. The bandwidth metric and the entropy metric ranked unsharp masking as the poorest enhancement technique. This is surprising as the Sobel function and unsharp masking are similar techniques. The variance metric ranked unsharp masking as the best technique, a result in sharp contrast to the rankings of the other metrics.

It is concluded from these results that the bandwidth metric and the entropy metric rank the techniques similarly to the observer's subjective fidelity criterion. It's understandable that the bandwidth metric would give similar rankings as the subjective criterion. Recall that the radial spatial frequencies chosen for summation in the bandwidth metric are chosen to coincide with the bandpass of the HVS.

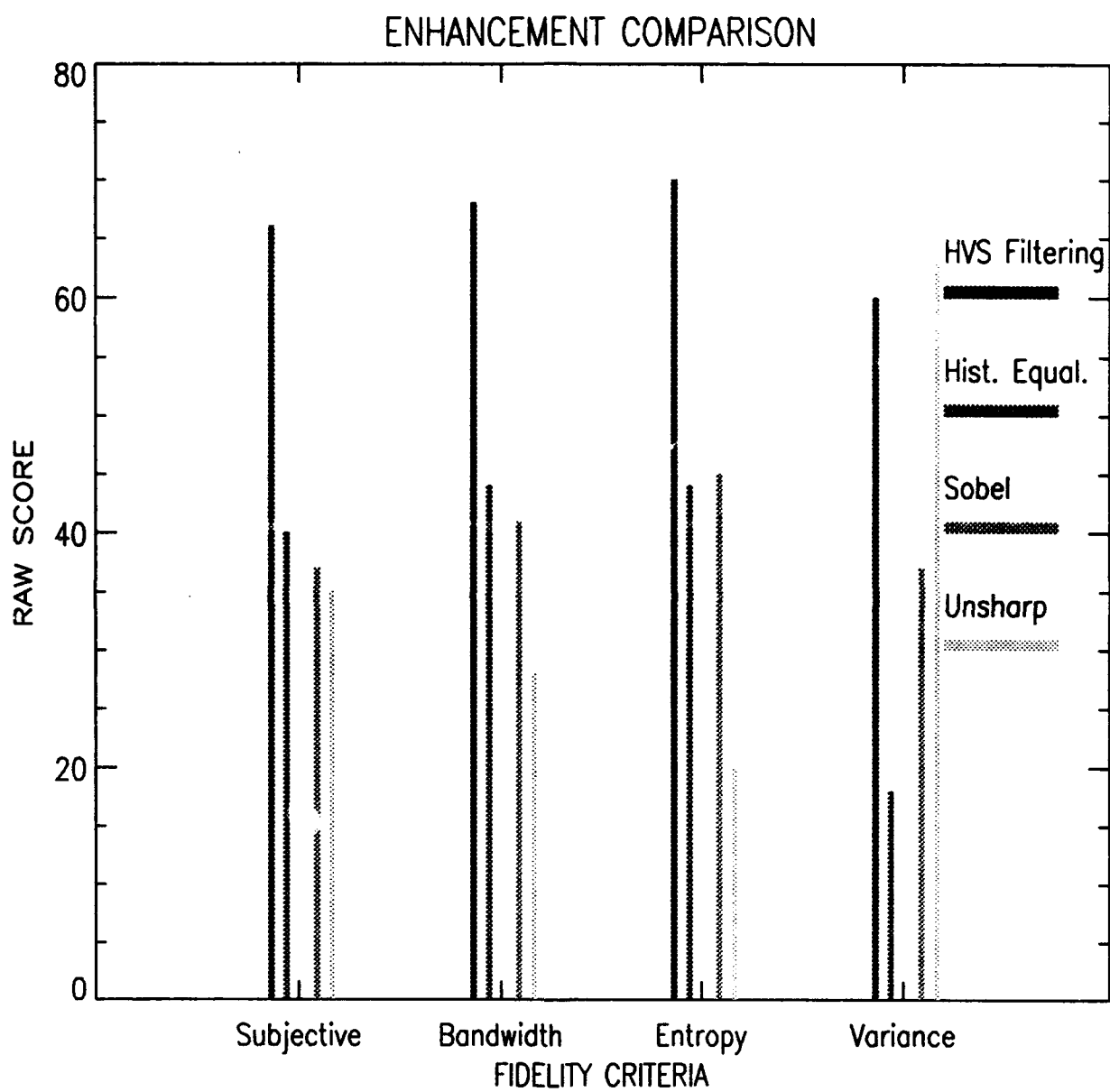


Figure 4.11 Comparison of the Various Enhancement Techniques by the Various Fidelity Criteria

V. Conclusion

5.1 Application of IDL Enhancement Routines

This research investigated four enhancement routines implemented in the IDL: human visual system (HVS) filtering, histogram equalization, Sobel function, and unsharp masking. HVS filtering preserves spatial frequencies in the passband of interest to the HVS. Histogram equalization can be considered a contrast enhancement technique; that is, it enhances the difference between light and dark portions of the image. The other two enhancement routines, Sobel function and unsharp masking, can be considered as edge enhancers. They highlight the location of edges in an image. Highpass filtering is the frequency domain equivalent of spatial domain edge enhancement.

All of the above mentioned techniques provided enhancement under certain conditions created during this research. These conditions included varying the atmospheric coherence diameters, (r_0), and the total number of photons per image, (\overline{K}), under which the reconstructed image data set was simulated.

It was found that HVS filtering provided enhancement under all conditions of simulation. Histogram equalization was found to be a good enhancer of images with low photon counts. This technique forced these images, which were generally dark, to have more bright elements, enhancing their contrast. However, it didn't help images with a high photon count, instead making them overly bright and washing out their features.

The Sobel function and unsharp masking provided good enhancement of images with high photon counts. They did not work well on images with low photon counts because the edges on such images were too poor to be enhanced. A future direction would be to enhance the contrast of low photon count images with histogram equalization prior to edge enhancement.

From knowing the photon count of an image, it is possible to select the best enhancement technique. Table 5.1 lists the best enhancement technique based on photon count.

Condition	Technique
all	HVS filtering
low photon count	histogram equalization
high photon count	Sobel function/ unsharp masking

Table 5.1 Technique Selection Matrix

5.2 *Fidelity Criteria*

This research applied objective criteria to the enhanced images in an effort to compare them with the reconstructed images. The objective criteria applied included the bandwidth metric, the entropy metric, and the variance metric.

If it's desired to replace the observer's subjective fidelity criterion with an objective criterion, then either the bandwidth metric or the entropy metric would be the metric of choice. They ranked the various enhancement techniques in the same order as did the subjective criterion.

5.3 *Avenues for Future Research*

This project was, by no means, an exhaustive study of satellite image enhancement. Time constraints limited the quantity of enhancement techniques which could

be explored. This research mapped out a small section of previously uncharted territory. The following is a list of potential follow-on research topics.

5.3.1 Topic: Better Unsharp Masking Technique. The unsharp masking technique used in this research really did nothing more than the Sobel function: it enhanced edges. A good unsharp masking technique preserves image contrast while enhancing edges. It does this by subtracting the blurred image from a scaled version of the original image. The unsharp masking routine used in this research lacked this scaling function. A properly chosen scale factor will preserve the contrast of the original image. A better unsharp masking routine was developed late in this research and is shown in Appendix C. It produced the image shown in Figure 4.10. However, time didn't permit the generation of a test matrix with this technique nor its evaluation by the quality assessments. Also, experiments should be conducted into finding an optimal window size for this technique. As the unsharp masked images for this research were generated automatically, all were smoothed using a 7 x 7 pixel window. This size was chosen after experimenting with it on a few images. It isn't optimal as evidenced by what it did to the OCNR5 image with $r_0 = 0.2$ and $\bar{K} = 10^4$.

5.3.2 Topic: Effects of Lower Photon Count. Only two different photon counts were used in the simulations leading to the data set used for this research: $\bar{K} = 10^4$ and 10^6 . A trend was clearly shown that for high photon counts, the edge enhancement techniques worked best. It would be interesting to lower the photon count to 10^3 , 10^2 , and 10, and see the effect on the histogram equalization technique.

5.3.3 Topic: Effects of Lower Atmospheric Coherence Diameter. Only three different atmospheric coherence diameters were used in the simulations leading to the data set used for this research: $r_0 = 20cm$, $10cm$, and $7cm$. No trend was clearly shown concerning r_0 . It would be interesting to lower the atmospheric coher-

ence diameter to 5cm, 4cm, and 3cm, and see the effect on the various enhancement techniques described in this research.

5.3.4 Topic: Combining Enhancement Techniques. In this research, the enhancement techniques were used individually. It would be interesting to see the effects of combining the techniques. For example, an image with poor contrast could be run through histogram equalization. Following that, one of the edge enhancement techniques could be applied. As a final step, it could be filtered by the MTF of the HVS. One of the problems to solve here is what to do if the edge enhancement technique gives a range of intensity values which exceed the range of the color table. The color table won't do justice to this expanded range. This problem could manifest itself as a gray, rather than a white, background when displaying an image negative.

5.3.5 Topic: Inverse Filtering with MTF of the HVS. This research accomplished linear filtering with the MTF of the HVS by multiplying the Fourier transform of the reconstructed image, I_r , by the MTF of the HVS to yield the Fourier transform of the enhanced image, I_e . Thus, I_e was given by:

$$I_e = I_r \times MTF. \quad (5.1)$$

Another way to use the MTF is as an inverse filter. If a transfer function is causing blurring of the image, the image can be sharpened by deconvolving the point-spread function from the measured image [18]. In the frequency domain, this would mean dividing the Fourier transform of the enhanced image by the MTF as follows:

$$I_e = \frac{I_r}{MTF}. \quad (5.2)$$

Appendix A. Spatial Domain Enhancement

; Capt James Treleaven
; 2 October 93

; This is an IDL procedure to automatically enhance reconstructed images.
; It accomplishes histogram equalization, Sobel function, and unsharp masking.
; It should be stored in a file titled: enhance.pro
; To compile, type: .run enhance
; To execute, type: enhance, file
; file should be a file containing the reconstructed image.

;;;;;;;;;;;;;;;;;

PRO enhance, file

; This section rotates reconstructed images into the same orientation
; as their true images. file should be a 256 x 256 unformatted,
; reconstructed image.

OPENR, unit, file, /f77_unformatted, /get_lun
a = FLTARR(256,256)
READU, unit, a
FREE_LUN, unit
a = ROTATE(a,4)
OPENW, unit, file + '.rcn', /f77_unformatted, /get_lun
WRITEU, unit, a
FREE_LUN, unit

;;;;;;;;;;;;;;;;;

; This section saves the reconstructed image after histogram equalization.

b = BYTE(a)
b = HIST_EQUAL(b)
b = FLOAT(b)
OPENW, unit, file + '.hequal', /f77_unformatted, /get_lun

```
WRITEU, unit, b
FREE_LUN, unit
```

```
;;;;;;;;;;;;;;;;;
```

```
;This section saves the reconstructed image after Sobel function.
```

```
c = SOBEL(a)
c = FLOAT(c)
OPENW, unit, file + '.sobel', /f77_unformatted, /get_lun
WRITEU, unit, c
FREE_LUN, unit
```

```
;;;;;;;;;;;;;;;;;
```

```
;This section saves the reconstructed image after unsharp masking.
```

```
d = FIX(a - SMOOTH(a,7))
d = FLOAT(d)
OPENW, unit, file + '.unsharp', /f77_unformatted, /get_lun
WRITEU, unit, d
FREE_LUN, unit
```

```
;;;;;;;;;;;;;;;;;
```

```
END
```

Appendix B. Human Visual System Filter

; Capt James Treleaven
; 4 November 93

; This is a portion of an IDL routine to compute a bandpass filter based
; on the MTF of the human visual system. For the complete code, see
; Capt Michael Roggemann, Dept. of Engineering Physics, School of
; Engineering, Air Force Institute of Technology, Wright-Patterson AFB,
; Ohio.

; image is the filename of the file containing the image to be filtered
; bandtype specifies the type of filter. In this case, it's bandpass.
; center is the desired center frequency of the filter.
; bandwidth is the desired bandwidth of the filter.
; order is the desired order of the filter.

imagesize = SIZE(image)
distfun = DIST(imagesize)
distfun(0) = 1e-4

IF(bandtype EQ 2) THEN \$; bandpass filter
filter = (distfun * distfun - center^2) / (distfun * bandwidth)
filter = (0.52+0.45*(distfun/center))*exp(-(filter ^ (2 * order) < 25))

Appendix C. A Better Unsharp Masking Routine

; Capt James Treleaven
; 4 November 93

; This is an IDL procedure to automatically unsharp mask a
; reconstructed image.
; It should be stored in a file titled: unsharp.pro
; To compile, type: .run unsharp
; To execute, type: unsharp, file
; file should be a file containing the reconstructed image.

PRO unsharp, file

OPENR, unit, file, /f77_unformatted, /get_lun
b = FLTARR(256,256)
READU, unit, b
FREE_LUN, unit
b = ROTATE(b,4)

; A is a scaling factor and may be changed as needed. It should
; be slightly greater than 1.0

A = 1.001

d = FIX(A*b - SMOOTH(b,7))

d = FLOAT(d)

OPENW, unit, file + '.unsharp', /f77_unformatted, /get_lun

WRITEU, unit, d

FREE_LUN, unit

TVSCL, d

END

Bibliography

1. Andrews, Harry C. "Multidimensional Rotations in Feature Selection," *IEEE Transactions on Computers*, 1045 - 1051 (September 1971).
2. Beavers, W.I., et al. "Speckle imaging through the atmosphere," *The Lincoln Laboratory Journal*, 2:207-228 (1989).
3. Cornsweet, T.N. *Visual Perception*. New York: Academic Press, 1970.
4. Davidson, Michael. "Perturbation Approach to Spatial Brightness Interaction in Human Vision," *Journal of the Optical Society of America*, 58:1300 - 1308 (September 1968).
5. DePalma, J.J. and E.M. Lowry. "Sine wave response of the visual system. Sine wave and square wave contrast sensitivity," *Journal of the Optical Society of America*, 52:328 - 335 (March 1962).
6. Gonzalez, Rafael C. and Richard E. Woods. *Digital Image Processing*. New York: Addison-Wesley Publishing Company, 1992.
7. Granrath, Douglas J. "The Role of Human Visual Models in Image Processing," *Proceeding of the IEEE*, 69:552 - 561 (May 1981).
8. Hall, Charles F. and Ernest L. Hall. "A Nonlinear Model for the Spatial Characteristics of the Human Visual System," *IEEE Transactions on Systems, Man, and Cybernetics*, SMC-7:161 - 170 (March 1977).
9. Kabrisky, Matthew. "An Introduction to a Model of the Human Visual System," *NAECON '73 Record*, 297 - 303 (1973).
10. Lee, Dave. *Objective Image Quality Metrics: Applications for Partially Compensated Images of Space Objects (Draft)*. MS thesis, AFIT/GSO/ENP/93D, School of Engineering, Air Force Institute of Technology(AU), Wright-Patterson AFB, OH, December 1993.
11. Mannos, James L. and David J. Sakrison. "The Effects of a Visual Fidelity Criterion on the Encoding of Images," *IEEE Transactions on Information Theory*, IT-20:525 - 536 (July 1974).
12. Nill, Norman B. "A Visual Model Weighted Cosine Transform for Image Compression and Quality Assessment," *IEEE Transactions on Communications*, COM-33:551 - 557 (June 1985).
13. Nill, Norman B. and Brian H. Bouzas. "Objective image quality measure derived from digital image power spectra," *Optical Engineering*, 31:813 - 825 (April 1992).
14. Pratt, William K. *Digital Image Processing*. New York: John Wiley and Sons, Inc, 1991.

15. Research Systems, Inc., 777 29th St., Ste. 302, Boulder, CO 80303. *IDL Reference Guide* (Version 3.0 Edition), January 1993.
16. Research Systems, Inc., 777 29th St., Ste. 302, Boulder, CO 80303. *IDL User's Library Online Documentation* (Version 3.0 Edition), January 1993.
17. Roggemann, M.C. "Optical performance of fully and partially compensated adaptive optics systems using least-squares and minimum variance phase reconstructors," *Computers and Electrical Engineering*, 18:451 - 466 (1992).
18. Roggemann, M.C., et al. "Linear reconstruction of compensated images: theory and experimental results," *Applied Optics*, 31:7429 - 7441 (10 December 1992).
19. Roggemann, Michael C. and Charles L. Matson. "Power spectrum and Fourier phase spectrum estimation by using fully and partially compensating adaptive optics and bispectrum postprocessing," *Journal of the Optical Society of America A*, 9:1525 - 1535 (September 1992).
20. Rome Air Development Center/OCSP, Griffiss AFB, NY 13441. *AMOS User's Manual*, September 1990.
21. Saghri, John A., et al. "Image quality measure based on a human visual system model," *Optical Engineering*, Volume 28, 28:813 - 818 (July 1989).

Vita

Captain James E. Treleaven was born on 31 December 1960 in San José, California. He graduated from Los Gatos High School in 1979 and enlisted in the U.S. Air Force, serving as a computer technician. He attended California State University, Sacramento, on scholarship from the Airman's Education and Commissioning Program, graduating with a Bachelor of Science in Electrical and Electronics Engineering in May 1987. He then attended Officer Training School, receiving a commission as a Second Lieutenant in October 1987. Upon graduation, he was assigned to Wheeler AFB, Hawaii, as a communications engineer with the 1843 Engineering and Installation Group. He entered the School of Engineering, Air Force Institute of Technology, in May 1992.

Permanent address: 147 Las Astas Dr., Los Gatos, California 95030

REPORT DOCUMENTATION PAGE			Form Approved OMB No. 0704-0188	
<small>Public reporting burden for this collection of information is estimated to average 1 hour per response, including the time for reviewing instructions, searching existing data sources, gathering and maintaining the data needed, and completing and reviewing the collection of information. Send comments regarding this burden estimate or any other aspect of this collection of information, including suggestions for reducing this burden, to Washington Headquarters Services, Directorate for Information Operations and Reports, 1215 Jefferson Davis Highway, Suite 1204, Arlington, VA 22202-4302, and to the Office of Management and Budget, Paperwork Reduction Project (0704-0188), Washington, DC 20503</small>				
1. AGENCY USE ONLY (Leave blank)		2. REPORT DATE December 1993		3. REPORT TYPE AND DATES COVERED Master's Thesis
4. TITLE AND SUBTITLE HUMAN VISUAL SYSTEM ENHANCEMENT OF RECONSTRUCTED SATELLITE IMAGES			5. FUNDING NUMBERS	
6. AUTHOR(S) James E. Treleaven, Captain, USAF				
7. PERFORMING ORGANIZATION NAME(S) AND ADDRESS(ES) Air Force Institute of Technology, WPAFB, OH 45433-6583			8. PERFORMING ORGANIZATION REPORT NUMBER AFIT/GEO/ENP/93D-04	
9. SPONSORING / MONITORING AGENCY NAME(S) AND ADDRESS(ES) Phillips Laboratory/LIMA 535 Lipoa Pkwy, Suite 500 Kihei, Maui, HI 96753			10. SPONSORING / MONITORING AGENCY REPORT NUMBER	
11. SUPPLEMENTARY NOTES				
12a. DISTRIBUTION / AVAILABILITY STATEMENT Approved for public release; distribution unlimited			12b. DISTRIBUTION CODE	
<small>(Maximum 200 words)</small> This research investigated the enhancement of satellite images. The goal was to develop and test a suite of image enhancement software routines to improve the quality of reconstructed images for the human visual system. The primary focus was to enhance satellite features. Enhancement was accomplished in both the spatial domain and the frequency domain. In the spatial domain, routines were developed to enhance image contrast and edges. In the frequency domain, a routine was developed using research into the human visual system. The transfer function of the human visual system was used to develop a filter for frequency domain enhancement. A data set of images was developed using software to simulate the image degradation caused by atmospheric turbulence and the randomness of the image measurement process. The parameters varied in the simulation were atmospheric coherence diameter and total photon count. The routines were applied to this data set and the results were evaluated by various image fidelity criteria. All enhancement routines provided enhancement dependent upon the parameters of the data set simulation. Contrast enhancement worked well when photon count was low. Edge enhancement worked well when photon count was high. The frequency domain filter worked well always.				
14. SUBJECT TERMS Image enhancement, human visual system, contrast enhancement, edge enhancement, histogram equalization, Sobel function			15. NUMBER OF PAGES 70	
			16. PRICE CODE	
17. SECURITY CLASSIFICATION OF REPORT Unclassified	18. SECURITY CLASSIFICATION OF THIS PAGE Unclassified	19. SECURITY CLASSIFICATION OF ABSTRACT Unclassified	20. LIMITATION OF ABSTRACT UL	